ITO/MoO_x/*a*-Si:H(i) hole-selective contacts for silicon heterojunction solar cells: degradation mechanisms and cell integration

Davide Sacchetto[1], Quentin Jeangros[2,3], Gabriel Christmann[1], Loris Barraud[1], Antoine Descoeudres[1], Jonas Geissbühler[1], Matthieu Despeisse[1], Aïcha Hessler-Wyser[2], Sylvain Nicolay[1], Christophe Ballif[1,2]

1 Centre Suisse d'électronique et de microtechnique (CSEM), PV-Center, Jaquet-Droz 1, CH-2000 Neuchâtel, Switzerland
2 Ecole Polytechnique Fédérale de Lausanne (EPFL), PV-lab, Rue de la Maladière 71b, CH-2002 Neuchâtel, Switzerland
3 Department of Physics, University of Basel, Klingelbergstrasse 82, Basel CH-4056, Switzerland

Molybdenum oxide is an efficient hole collector for silicon solar cells. However, its optoelectronic properties deteriorate during cell manufacturing. To assess this issue, the optoelectronic properties and microstructure of molybdenum oxide-based hole contacts are evaluated at different steps of the manufacturing process. Molybdenum oxide becomes more absorbing as it reduces when placed in contact with hydrogenated amorphous silicon, triggering the formation of a 2-nm thick SiO_x layer, and when annealed after exposure to the plasma used to sputter the transparent conductive oxide. These changes in the contact properties result in a barrier that impede hole transport when measuring *I-V* characteristics at room temperature. Nonetheless, cells still reach an efficiency of up to 20.7% when using a front metal electrode screen-printed at 210 °C (21.7% for reference cells). Above 60°C, both molybdenum oxide-based and reference cells exhibit the same efficiency as this barrier to hole transport vanishes.

I. INTRODUCTION

In the past decade, the efficiency of silicon heterojunction (SHJ) solar cells has been improving steadily, with record values now exceeding 25% for front and back contacted solar cells [1]. In the conventional SHJ design, surface passivation and hole collection is obtained by the deposition on the c-Si wafer of a bilayer composed of intrinsic and doped hydrogenated amorphous silicon (a-Si:H(i) and a-Si:H(p), respectively). This stack is then capped by a transparent conductive oxide (TCO) to guarantee an efficient light coupling into the device and a lateral current flow to the metal contacts. These thin films need to be carefully optimized, especially at the front side of the cell, or they may cause undesired optical and electrical losses. For example, a sufficiently thick and highly doped a-Si:H(p) layer is needed to guarantee a good hole collection from the wafer and a low specific contact resistivity with the overlying TCO. However, this may lead to undesired optical losses [2] and a degradation of the passivation of the c-Si surface [3], [4].

In this context, transition-metal oxides (TMOs) such as MoO_x, WO_x, VO_x, and NiO_x have been recently proposed as possible alternatives to the a-Si:H(p) layer in SHJ cells [5]–[8]. They combine a wide bandgap with a high work-function and can thus provide a good hole selectivity. Promising results were recently reported for MoO_x integrated in SHJ devices [6], [7]. In Ref. [7], an efficiency of 22.5% was achieved by employing a ~7 nm MoO_x layer that was thermally evaporated on the a-Si:H(i) buffer layer and subsequently capped by highly conductive hydrogen-doped indium oxide (IO:H). Yet, high efficiencies could be reached only at the expense of the overall process simplicity. Indeed, the conventional screen-printed Ag metallization could not be used as the performance of the cells dropped when using the usual contact curing temperature of ~200 °C. In fact, 130 °C was found to be the upper processing temperature for this cell design. To circumvent this issue, a room temperature Cu electroplating metallization process was required to reach the high efficiency reported above [9].

The difficulty of integrating MoO_x in a SHJ using standard process parameters stems from the sensitivity of its chemistry to the manufacturing parameters. MoO_x can quickly become sub-stoichiometric (x <3) when reacting with *i)* charged ions such as H^+ [10], [11], *ii)* adsorbed H_2O molecules when irradiated with UV light [12] and *iii)* with neighboring layers that present a higher oxygen affinity. All these effects are potentially accelerated at high temperature. These changes in the MoO_x chemistry are likely to occur when integrating it in a SHJ as it:

i) may react with H-containing a-Si and TCO layers [13], which may also result in the formation of a hole-blocking layer on the TCO side of the interface at ~200 °C [7],
ii) is exposed to both UV radiations [14] and (if the TCO is hydrogenated) H_2O vapor [15] during TCO sputtering, and
iii) is in contact with Si, which may trigger the oxidation of Si over 2-3 nm [16].

These effects hinder the hole extraction capabilities of MoO_x as its work function decreases with oxygen content, a trend also measured when studying WO_x thin films [17]. As reported by Bivour and co-workers, this reduction in the work function becomes particularly severe when MoO_x-based SHJ cells are annealed at temperatures on the order of 180 °C [6].

The points raised above highlight the need for a careful analysis of the TCO/MoO_x and MoO_x/a-Si:H(i) interactions to enable a successful integration of this TMO in SHJs. In that regard, this work presents a detailed assessment of the optical absorption, electrical conductivity and microstructure of these films in different stack configurations and at different temperatures. The aim is to understand the key features governing the overall properties of MoO_x-based SHJ contacts during cell manufacturing. Then, solar cell results that employ an optimized carrier selective MoO_x/a-Si:H(i) contact stack are discussed and compared to the conventional a-Si:H(p)/a-Si:H(i) front passivating contact.

II. EXPERIMENTAL DETAILS

For solar cell fabrication, high quality 4 Ω cm n-type <100> float zone wafers were textured in a KOH solution and subsequently cleaned. The remaining chemical oxide was then stripped off in 5% diluted HF, immediately followed by the deposition of a 10-nm intrinsic a-Si:H(i) film by plasma enhanced chemical vapor deposition (PECVD) on both wafer sides. The electron collector was realized by subsequent plasma deposition of a 10-nm thick n-doped a-Si:H film on the rear side for all the devices. For hole collection, a ~10-nm thick MoO_x layer was thermally evaporated from a MoO_3 source at room temperature with a growth rate of 0.5 Å s^{-1} at a base pressure of $3 \cdot 10^{-6}$ mbar. Alternatively, a 10-nm thick p-doped a-Si:H film was deposited by PECVD as a reference. The thin film thicknesses of a-Si:H and MoO_x layers were measured on cleaned and flat glass substrates by fitting a Tauc-Lorentz model to spectroscopic ellipsometry data (α-SE Woollam). The thicknesses of ITO, Ag and Al layers deposited on glass were measured with a mechanical profiler. The rear electrode consists of an ITO/Ag stack deposited by DC magnetron sputtering, while the front electrical contacts are fabricated by depositing 110 nm of hydrogen-free ITO (65 nm on textured Si) and a screen-printed Ag grid. The sputtering of ITO (front and rear) was performed at a substrate temperature of 80°C in an Ar/O_2 plasma, while the Ag at the rear was sputtered in pure Ar at 60°C. The low temperature Ag paste (Namics N10) was cured with cumulative annealing steps, increasing the temperature up to 210°C with steps of 10 minutes. The Ag paste line resistance was calculated from 5 cm long lines on textured substrates. The resulting 2x2 cm^2 solar cells were then characterized by light *I-V* (Wacom solar simulator, Keithley 2601A sourcemeter) and external quantum efficiency (EQE) measurements. Photoconductivity decay measurements were carried out with a Sinton Consulting WTC-100 apparatus to evaluate the surface passivation properties, for which symmetric test structures were specially designed. The optical absorption of individual a-Si:H(i), MoO_x, ITO films and stacks deposited on borosilicate glass was measured using a spectrophotometer (Lambda 950, Perkin Elmer), equipped with an integrating sphere. The electrical contacts for dark conductivity

measurements were fabricated by thermal evaporation of 300-nm thick Al strips through a shadow mask. The microstructure of ITO/MoO_x/a-Si:H(i) deposited on mirror-polished c-Si <111> wafers was characterized by means of high-resolution TEM (HRTEM) and high-resolution scanning TEM (HRSTEM) high-angle annular dark-field (HAADF) imaging in an FEI Titan Themis transmission electron microscope (TEM) operated at 200 kV. The latter technique was combined with electron energy-loss spectroscopy (EELS) using a Gatan GIF Quantum ERS high-energy resolution spectrometer and energy-filter to assess the spatial distribution of elements within the stack. The STEM EELS convergence and collection semi-angles were 28 mrad and 47.3 mrad, respectively, while the beam current was set to 200 pA. The thin TEM lamellae were extracted using the conventional focused ion beam (FIB, here a Zeiss Nvision 40 crossbeam) lift-out method and thinned to their final thickness with a Ga^+ acceleration voltage of 5 kV.

III.RESULTS

A. Optical Properties of ITO/MoO_x/a-Si:H stacks

The optical absorptance of single layers and stacks of as-deposited a-Si:H(i), MoO_x and ITO films are compared before and after annealing in Fig. 1. Individual as-deposited MoO_x films are transparent up to 2 eV, hence indicating a composition close to the stoichiometric MoO_3 phase [18]. The a-Si:H(i) layer is also transparent when deposited on glass. On the other hand, the as-deposited MoO_x/a-Si:H(i) bilayer has a broad absorption peak at 1.4 eV, which does not change upon annealing. This observation tends to indicate that the Mo^{6+} cations may already reduce once evaporated on the a-Si:H(i) layer, presumably due to the presence of H in this second layer. Indeed, a report by Borgschulte *et al.* demonstrates that MoO_x reduces already at room temperature when in contact with atomic hydrogen [19]. The same effect was reported for WO_x/a-Si:H(i) interfaces [17]. A similar absorption peak appears at 1.4 eV when annealing individual MoO_x layers in air, in agreement with the observations of Refs. [14], [18]. Mo cations may reduce due to the desorption loosely bound O, an effect that might be more significant than O_2 adsorption, dissociation and diffusion into the film in this low temperature range (an effect observed e.g. in SnO_2 thin films [20]). The effects of plasma luminescence and ion bombardment during sputtering of the TCO become detrimental only after annealing, with a loss of transparency of 2 % absolute measured in the range 1 to 2 eV (Fig. 1b). This increase in absorptance occurs even if the MoO_x layer is exposed only during 1 s to the plasma employed for ITO deposition. Literature indicates that MoO_x may reduce when exposed to a N_2 or Ar plasma (O is preferentially sputtered when exposed to an Ar plasma [21] and when exposed to UV radiations [22]). These plasma-induced processes may damage the structure of the hole contact stack (e.g. by disturbing locally both the MoO_x and a-Si:H(i) atomic structure), but these do not appear to result in a reduction of the Mo cations unless the temperature is increased. O (from the MoO_x) or H (from the a-Si:H) may be more mobile and hence more likely to desorb or diffuse with temperature after plasma irradiation, overall resulting in a further reduction of the Mo cations. The subsequent sputtering of the ITO layer does not induce additional optical losses at 1.4 eV when compared to the stack exposed 1 s to the plasma.

Overall, as an annealing step is necessary to manufacture SHJ cells, both the presence of an a-Si:H(i) layer and the TCO sputtering process will reduce the optical transparency of the MoO_x layer. Nonetheless, ITO/MoO_x/a-Si:H(i) stacks have a lower absorptance when compared to an ITO/a-Si:H(p)/a-Si:H(i) contacts due to the increased MoO_x transparency when compared to that of a-Si:H(p) (discussed later, see Fig. 5a).

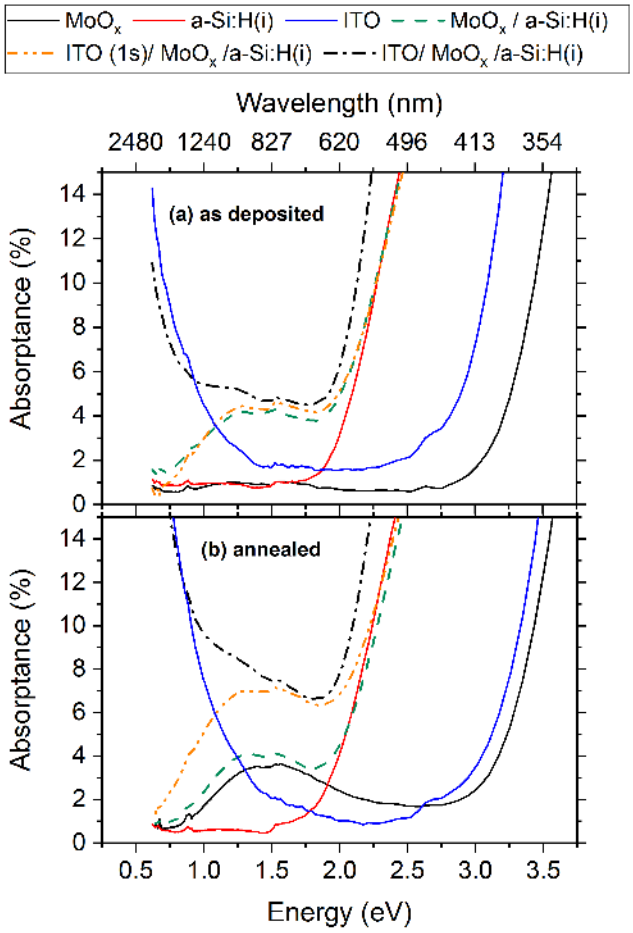

FIG. 1. Optical absorptance of MoO_x, ITO and a-Si:H(i) films deposited separately or sequentially on borosilicate glass measured (a) before and (b) after annealing at 180°C in air during 20 min.

B. Electrical Properties of of ITO/MoO_x/a-Si:H stacks

To investigate the electrical properties of MoO_x and MoO_x/a-Si:H(i) layers on glass, coplanar dark conductivity measurements (σ_{dark}) were performed from 180 to 25 °C in 1 mbar of inert N_2 atmosphere (Fig. 2). To minimize the effect of annealing in N_2 during the measurement, these samples were pre-annealed in air at 180°C for 20 min before the dark conductivity measurements to stabilize the layers. The electrical conductivity of MoO_x films increases as Mo cations reduce, hence making the layer less transparent as shown in Fig. 1 [12]. Indeed, as shown in Fig. 2, the σ_{dark} of MoO_x of layers deposited on 10 nm of a-Si:H(i) is more than 1 order of magnitude larger than that of MoO_x films deposited on glass. As the σ_{dark} of a-Si:H(i) films is typically only ~10^{-8} $Ohm^{-1}\cdot cm^{-1}$ [23], the increased conductivity should originate from the MoO_x layer, hence confirming the reduction of the Mo cations when in contact with a-Si:H(i) [16], [24]. Interestingly, the values of dark conductivity for MoO_x layers are larger than those of a-Si:H(p)/a-Si:H(i) stacks, indicating better electrical transport in MoO_x.

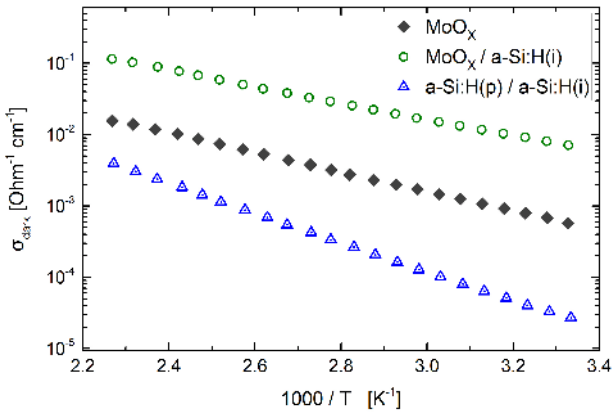

FIG. 2. Dark conductivity of MoO_x, MoO_x/a-Si:H(i) and a-Si:H(p)/a-Si:H(i) stacks deposited on glass.

C. Structural Properties of ITO/MoOx/a-Si:H stacks

To characterize the interfaces of the MoO_x-based SHJ contact, ITO/MoO_x/a-Si:H(i) stacks were investigated by high-resolution (S)TEM before and after annealing (Fig. 3). The MoO_x layer is found to be amorphous before and after annealing. A 2-nm amorphous O-rich Si layer is observed at the a-Si:H(i)/MoO_x interface in both cases, highlighting the presence of a SiO_x interlayer. This oxygen-rich layer may originate either from the oxidation in air of a-Si:H during the transfer from the PECVD reactor to the evaporator (here exposure to air of ~30 min) or from a transfer of O^{2-} from the MoO_x layer to the a-Si:H(i). As air exposure of a-Si:H(i) thin films is known to form a SiO_x layer of only a few Å (even after days of oxidation in air at room temperature [25], [26]), a significant part of the 2 nm of oxide observed here is thought to arise from the interaction of a-Si:H(i) with MoO_x, as already observed in Refs. [16], [17]. In agreement with the data shown in Figs. 1 and 2, it is indeed likely that MoO_x reduces and a-Si:H(i) oxidizes when in contact due to the higher oxygen affinity of Si [27]. As the SiO_x layer does not appear to thicken further when annealing at 180 °C (Fig. 3b), its growth kinetics seems controlled, at least in this temperature range, by the energetics of the MoO_x/a-Si:H(i) interface rather than by a thermally activated diffusion process [28]. The electric-field that forms at the interface appears to drive the migration of O^{2-} to the Si side [29], [30]. The fact that

MoO_x and a-Si:H(i) do not interact further when annealing at 180 °C is in agreement with the optical data shown in Fig. 1 (see MoO_x/a-Si:H(i) stacks before and after annealing). As reported for the case of MoO_3 deposited on metals [29], this reduction of the Mo cations at the expense of Si increases the conductivity of MoO_x layer compared to when deposited on glass (see Fig. 2).

A previous TEM analysis of a SHJ front stack composed of IO:H, MoO_x and a-Si:H(i) suggested the formation of an interlayer at the MoO_x/IO:H interface during annealing [7]. In contrast, the ITO/MoO_x interface appears here largely unaffected by a temperature of 180 °C (Fig. 3b): the Mo $M_{2,3}$ EELS edges are seen to decrease quickly across the interface, with the In $M_{4,5}$ intensity increasing simultaneously (see colored regions Fig. 3). This difference is likely to arise from the use of a hydrogenated TCO in [7], as H may have migrated across the interface with MoO_x during annealing. It should be mentioned that the ITO/MoO_x interface appears here to be slightly more diffuse in projection in the as-deposited state when compared to the annealed state (see small overlap in colored regions in Fig. 3a). This is likely due to a combination of a small roughness of the MoO_x layer, which in projection appears as ITO/MoO_x intermixing, and a difference in FIB-prepared sample thickness (~60 nm for the as-deposited specimen compared to ~30 nm after annealing, estimated from the low-loss EEL spectrum using the log-ratio method [31]). The increase in absorptance of the a-Si:H(i)/MoO_x/ITO stack after annealing observed in Fig. 1 is not linked to the formation of an interlayer between MoO_x and ITO as that observed in Ref. [7]. As discussed in Section III.D, it appears more likely that MoO_x reduces uniformly due to a combination of plasma exposure and temperature. While an analysis of the fine structure of the Mo $M_{3,2}$ and O K edges could provide this information [32], no noticeable changes could be measured here, presumably due to a lack of sensitivity of the EELS data. Furthermore, it should be mentioned that MoO_x was found to crystallize under the electron beam when acquiring core-loss STEM EELS data, an effect that may influence its stoichiometry [33], [34].

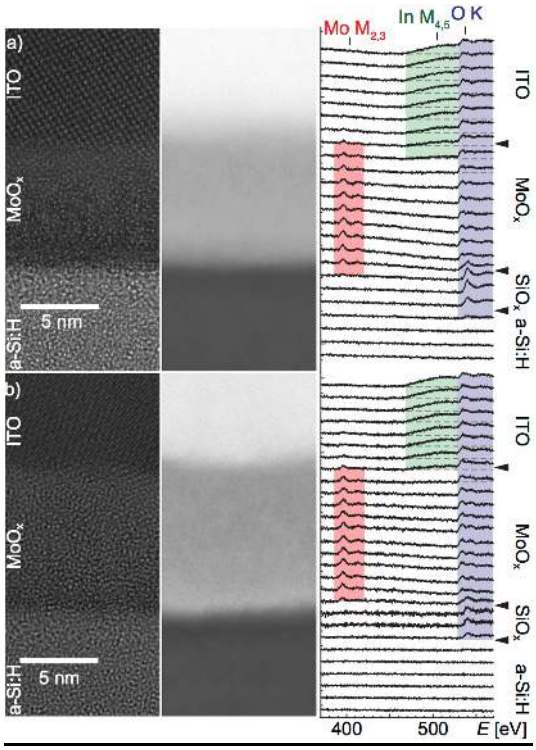

FIG. 3. (From left to right) high-resolution TEM, STEM HAADF micrographs and corresponding EEL spectra of the ITO/MoO_x/a-Si:H(i) stacks (a) as deposited and (b) annealed at 180°C during 20 min. The TEM and STEM EELS data were taken from different regions of the sample as the MoO_x layer was observed to crystallize under the electron beam when acquiring EELS spectra. The spectral regions where the Mo $M_{2,3}$, In $M_{4,5}$ and O K edges are detected are colored in red, green and blue, respectively (see [35] for the EELS edges references).

D. Interface passivation with MoO_x/a-Si:H

Fig. 4 shows the carrier lifetime of symmetric test structures consisting of MoO_x/a-Si:H(i) or a-Si:H(p)/a-Si:H(i) before and after ITO deposition and annealing.

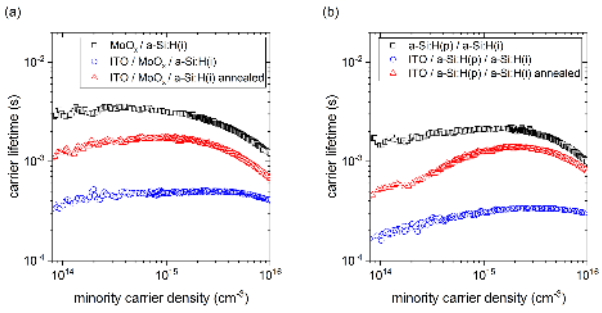

FIG. 4. Carrier lifetime versus minority carrier density of (a) MoO_x/a-Si:H(i) and (b) a-Si:H(p)/a-Si:H(i) symmetric structures following MoO_x and reference cell fabrication flows, respectively. The carrier lifetime was measured before (black squares), after ITO deposition (blue circles) and after annealing in air at 180°C for 20 min (red triangles).

In either case, the carrier lifetime is much lower after ITO sputtering, as metastable defects are created in the a-Si:H(i) layer. This affects its c-Si surface passivation properties, as also observed in standard SHJ solar cells [36]. The passivation quality is partially recovered by annealing the

samples at 180°C for 20 minutes. A small carrier lifetime is observed at low injections for the a-Si:H(p)/a-Si:H(i) reference, likely due to an incomplete recovery of sputtering defects during annealing. Consequently, the c-Si surface potential – and thus band-bending in the Si wafer – is reduced, increasing carrier recombination at low injection [37]. Remarkably, this 'tailing' of the lifetime curve is less pronounced for MoO_x based samples, indicating that the c-Si surface potential is better maintained. This difference indicates that MoO_x screens better the c-Si surface potential from the work function of the TCO, when compared to a-Si:H(p). The improved passivation of the MoO_x-based symmetric structures shown in Fig. 4 enables to thin down the a-Si:H(i) layer from 10 nm (reference thickness) to 7 nm (thin a-Si:H(i)) at the p-side and thereby potentially reducing parasitic absorption and also improving carrier transport, as it will be discussed in the next sections.

E. Annealing resilience of SHJs with ITO/MoO_x/a-Si:H

Generally, an annealing process is necessary in SHJ solar cell production to *i)* reduce the line and contact resistances of the printed Ag paste, *ii)* recover the passivation damage of the amorphous Si layers induced by TCO sputtering and *iii)* improve the opto-electrical properties of the TCOs integrated in the final device. To find the ideal trade-off between these different technological requirements and the fact that MoO_x-based cells may degrade under annealing, the impact of annealing (10 min steps at increasing temperatures of 100 °C, 130 °C, 180 °C and 210 °C) was tested on final devices. For this, SHJ cells with the proposed ITO/MoO_x/a-Si:H(i) stack, using the 7 and 10 nm a-Si:H(i) layers, were fabricated and compared to a reference SHJ cell that employs a conventional front side structure. In all cases, a Ag paste screen printing metallization process was used to form the metal lines.

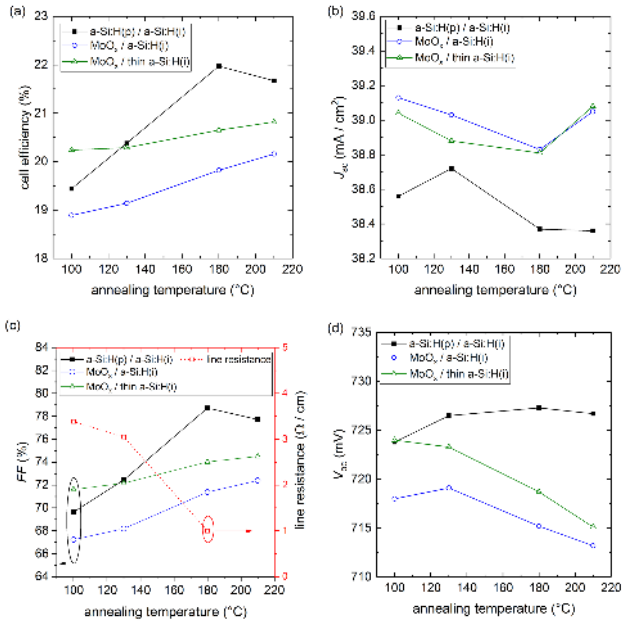

FIG. 5. Light *I-V* upon cumulative annealing conditions: (a) efficiency, (b) J_{sc}, (c) *FF* (left axis) with Ag paste line resistance (red curve, right axis) and (d) V_{oc}. Annealing is performed in air starting from 10 min at 100 °C before incrementally increasing the curing temperature up to 210 °C. In all cases the *FF* increases with the annealing temperature and follows the reduction of line resistance.

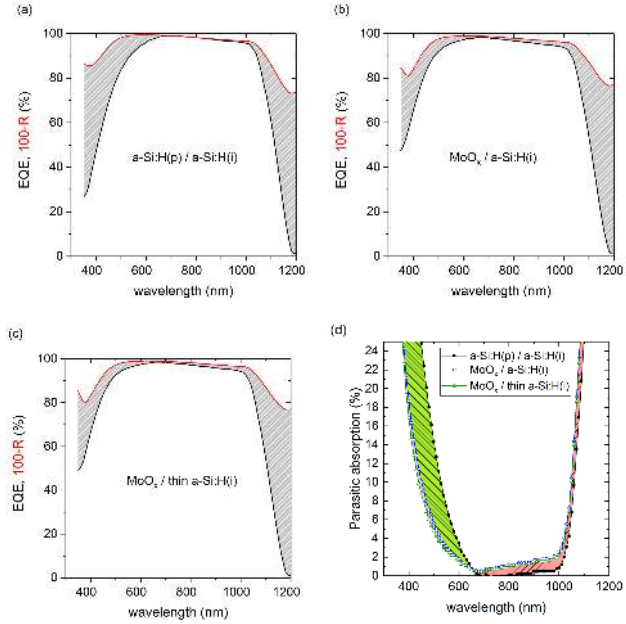

FIG. 6. EQE and 100-R of cells with different hole-collecting stacks after the annealing at 210°C: (a) a-Si:H(p)/a-Si:H(i) reference; (b) MoO_x/ a-Si:H(i); (c) MoO_x/ thin a-Si:H(i). (d) Parasitic optical absorption calculated from the EQE and reflectivity of the cells. In the table inset, the J_{sc} values are obtained by integrating the EQE data in the different regions of the spectra.

Figure 5a shows that at 100 °C the overall efficiency of the MoO_x/thin a-Si:H(i) cell is superior to that of the reference device. This is mainly due to the higher optical transparency at the front, leading to an increased short circuit current (J_{sc}) (see Fig. 5b), and to a larger fill factor (*FF*, Fig. 5c). It is also observed that the thickness of the a-

Si:H(i) layer does not significantly impact the optical transparency of MoO_x-based cells, as these have similar J_{sc} (Fig. 5b) and external quantum efficiencies (EQE, Fig. 6).

By integrating the area between the non-reflected light (100-R, R is the reflectance, red curves in Fig. 6a-c) and the EQEs (black curves of Fig. 6a-c) at UV, visible and near infrared wavelengths, the parasitic optical losses can be evaluated (Fig. 6d). Interestingly, the cells that include MoO_x have a lower parasitic absorption than the reference cell at the UV and visible wavelengths (green shaded area in Fig. 6d) but a worse performance at longer wavelengths (red shaded area in Fig. 6d). This is another indication that the optical properties of the cells are limited by the MoO_x absorptance in the near infrared region (in the 700-1000 nm range, corresponding to 1.2-1.8 eV), confirming the observations of Section III.A. After the first annealing at 100°C, the *FF* (Fig. 5c, left axis) of the MoO_x/thin a-Si:H(i) cells is significantly higher than these including a MoO_x/thick a-Si:H(i) stack as carrier transport is increased in the former case. Indeed, it has been shown that thicker a-Si:H layers lead to lower *FF*s if a sufficient degree of surface passivation is obtained [2]. Curing the solar cells at higher temperatures leads to an improved *FF* and, for the reference cell, it follows the improved conductivity of the Ag-paste (see Fig. 5c). For MoO_x cells, however, this *FF* improvement is less pronounced. As inferred from Figs. 1 and 2, annealing causes a reduction of MoO_x. As the work function of MoO_x is known to decrease with its oxidation state [14], [29], the band alignment between a-Si:H(i) and MoO_x changes during annealing and decreases the hole extraction capabilities of the stack, as observed by Bivour *et al.* [6].

The open circuit voltage (V_{oc}) of MoO_x-based cells decreases upon annealing (Fig. 5d). This effect is not related to a change in passivation (Fig. 4) but rather, as it will be shown in the next section, a consequence of an S-shape in the *I-V* characteristics around the V_{oc} when measured at 25 °C (Fig. 7a).

F. Temperature dependence of cell parameters

To assess further these losses in V_{oc} and *FF* of cells annealed at 210 °C, *I-V* curves were measured as a function of temperature from 25 to 85 °C. From these measurements, it appears that the S-shape of the MoO_x cells flattens when increasing the temperature from 25 to 85 °C (Fig. 7a). At T < 60 °C, the non-linear behavior of the $V_{oc}(T)$ of MoO_x cells indicates a non-optimal band alignment and hence a hindered carrier extraction (Fig. 7b). On the other hand, reference ITO/a-Si:H(p)/a-Si:H(i) cells do not exhibit any S-shape and their V_{oc} decreases linearly at -1.8 mV °C^{-1} from 25 to 85 °C (Fig. 7b). A broad *FF* maximum is observed at ~60°C for cells that include MoO_x (Fig. 7c, blue and green curves). On the other hand, the *FF* of reference cells (black curve) monotonically decreases with temperature. To investigate the origin of the *FF* losses in MoO_x cells, the series resistance R_{serie} of the solar cells is extracted from *I-V* data at different illuminations with the method described in [38]. From that analysis, it appears that the electrical losses at low temperature are induced by the presence of a large series resistance (Fig. 7d). At temperatures > 60 °C, the series resistance of MoO_x-based cells decreases and approaches that of the reference cells.

It hence appears that a potential barrier for holes is present at the MoO_x/a-Si:H interface < 60 °C. This effect arises because *i)* the hole extraction capabilities of the MoO_x layer worsen as its work function decrease due to a reduction of Mo cations to an oxidation state lower than +6 during cell processing (as inferred from Figs. 1 and 2) and *ii)* a resistive SiO_x interlayer forms at the MoO_x/a-Si:H(i) interface during deposition due to the higher affinity of Si towards O (Fig. 3). As demonstrated by Seif and co-workers [39], a thin passivating a-SiO_x(i) layer placed between the c-Si wafer and the a-Si:H(p) contact forms a barrier that impedes hole collection up to an operation temperature of 50 °C. Furthermore, the *FF(T)* evolution reported in [39] is similar to that measured here in Fig. 7c with a broad maximum reaching ~75% at 60°C. These similarities indicate that the SiO_x interlayer observed here probably influences hole transport across the contact.

Overall, the hole collection capabilities of the MoO_x contact improves above 60 °C, which means that MoO_x-based cells lose efficiency less rapidly with temperature compared to reference cells (see Fig. 7e). While the reference ITO/a-Si:H(p)/a-Si:H(p) cells have a higher efficiency than MoO_x-

based cells at 25 °C, even when using a thinner a-Si:H(i) layer for the latter case (21.7% compared to 20.7%, respectively), their efficiencies eventually match when operating the cells above 60 °C (Fig. 7b), a condition that is often reached in the field. These promising results are enabled by thinning the a-Si:H(i) by 3 nm as the MoO_x layer protects more efficiently the intrinsic passivating layer from sputter damage when compared to the conventional a-Si:H(p). This optimization of the a-Si:H(i) layer enables to gain > 0.5% absolute in efficiency when compared to cells that employ the baseline intrinsic layer thickness due to an improvement in the fill factor of about 2%.

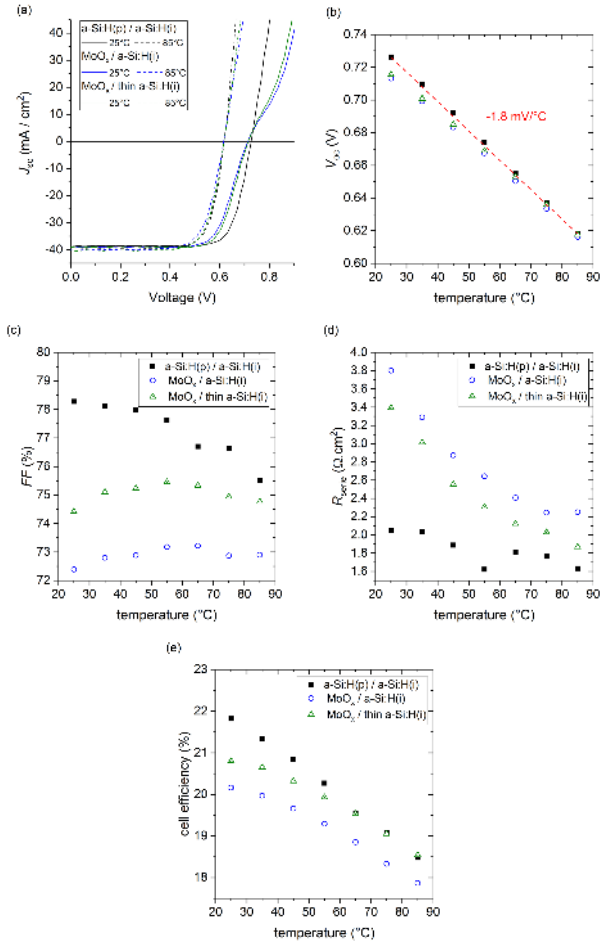

FIG. 7. (a) *I-V* characteristics of a-Si:H(p)- and MoO_x-based SHJ solar cells measured from 25°C to 85°C after annealing at 210°C. (b) $V_{oc}(T)$ showing the linear decrease of V_{oc}= -1.8 mV/°C with operating temperature and sub-linear decrease for MoO_x-based cells. (c) *FF*, (d) series resistance (R_{serie}) of the cells in the range 25 to 85°C and (e) cell efficiency

IV. CONCLUSIONS

The optoelectronic properties of single- or multi-layer stacks of a-Si:H(i), MoO_x and ITO were investigated before and after annealing at the temperatures required for SHJ manufacturing. The optical absorption MoO_x increases strongly when it is deposited on a-Si:H(i) and when annealed after exposure to the plasma employed for TCO sputtering. Moreover, the dark conductivity of MoO_x/a-Si:H(i) is larger than that of as-deposited MoO_x on glass, which indicates that Mo reduces when in contact with a-Si:H(i). This affects the hole collecting capabilities of this layer as it reduces its work function. Furthermore, a resistive SiO_x layer forms on the a-Si:H(i) side of the interface, with O originating from the MoO_x. Both effects create a barrier for holes that limit the cell properties at room temperature. While this barrier limits the efficiency of MoO_x-based cells that are manufactured using a standard industrial metallization process at 210 °C, an efficiency of 20.7 % is still reached (21.7 % for reference a-Si:H(p) cells). MoO_x screens more efficiently the underlying a-Si:H(i) from sputter damage and hence enables to thin down this latter layer to gain notably in fill factor. Furthermore, hole extraction is greatly improved above 60°C as the potential barrier for hole transport vanishes, with MoO_x- and a-Si:H(p)-based cells showing the same efficiency above this temperature.

ACKNOWLEDGEMENT

The interdisciplinary Centre for Electron Microscopy at EPFL is gratefully acknowledged for FIB and TEM access. This project has received funding from the European Union's Horizon 2020 research and innovation program under grant agreement No 641864 and by CTI TACOS project n°16637.2 PFNM-NM. Stephanie Essig and Stefaan de Wolf are acknowledged for fruitful discussions.

References

[1] K. Yamamoto, D. Adachi, H. Uzu, T. Uto, T. Irie, M. Hino, Kanematsu, H. Kawasaki, K. Konishi, R. Mishima, K. Nakano, T. Terashita, T. Yoshikawa, M. Ichikawa, T. Kuchiyama, T. Suezaki, T. Meguro, N. Nakanishi, M.

Yoshimi, D. Schroos, N. Valckx, N. Menou, and J. L. Hernández, “Progress & Challenges in Thin-Film Silicon Photovoltaics: Heterojunctions & Multijunctions,” in *EUPVSEC*, 2015.
[2] Z. C. Holman, A. Descoeudres, L. Barraud, F. Z. Fernandez, J. P. Seif, S. De Wolf, and C. Ballif, “Current Losses at the Front of Silicon Heterojunction Solar Cells,” *IEEE J. Photovoltaics*, vol. 2, no. 1, pp. 7–15, 2012.
[3] S. De Wolf and M. Kondo, “Nature of doped a-Si:H/c-Si interface recombination,” *J. Appl. Phys.*, vol. 105, no. 103707, pp. 1–6, 2009.
[4] G. Nogay, J. P. Seif, Y. Riesen, A. Tomasi, Q. Jeangros, N. Wyrsch, F.-J. Haug, S. De Wolf, and C. Ballif, “Nanocrystalline Silicon Carrier Collectors for Silicon Heterojunction Solar Cells and Impact on Low-Temperature Device Characteristics,” *IEEE J. Photovoltaics*, vol. 6, no. 6, pp. 1654–1662, Nov. 2016.
[5] L. G. Gerling, S. Mahato, A. Morales-vilches, G. Masmitja, P. Ortega, C. Voz, R. Alcubilla, and J. Puigdollers, “Solar Energy Materials & Solar Cells Transition metal oxides as hole-selective contacts in silicon heterojunctions solar cells,” *Sol. Energy Mater. Sol. Cells*, vol. 145, pp. 109–115, 2016.
[6] M. Bivour, J. Temmler, H. Steinkemper, and M. Hermle, “Solar Energy Materials & Solar Cells Molybdenum and tungsten oxide : High work function wide band gap contact materials for hole selective contacts of silicon solar cells,” *Sol. Energy Mater. Sol. Cells*, vol. 142, pp. 34–41, 2015.
[7] J. Geissbühler, J. Werner, S. M. D. Nicolas, L. Barraud, A. Hessler-Wyser, M. Despeisse, S. Nicolay, A. Tomasi, B. Niesen, S. De Wolf, and C. Ballif, “22.5% efficient silicon heterojunction with molybdenum oxide hole collector,” *Appl. Phys. Lett.*, vol. 107, no. 8, p. 81601, 2016.
[8] R. Islam, P. Ramesh, J. H. Nam, and K. . Saraswat, “Nickel Oxide Carrier Selective Contacts for Silicon Solar Cells,” in *Photovoltaic Specialist Conference (PVSC)*, 2015, pp. 1–4.
[9] J. Geissbühler, S. De Wolf, A. Faes, N. Badel, Q. Jeangros, A. Tomasi, L. Barraud, A. Descoeudres, M. Despeisse, and C. Ballif, “Silicon heterojunction solar cells with copper-plated grid electrodes: Status and comparison with silver thick-film techniques,” *IEEE J. Photovoltaics*, vol. 4, no. 4, pp. 1055–1062, 2014.
[10] C. G. Granqvist, “Handbook of Inorganic Electrochromic Materials,” Amsterdam, The Netherlands: Elsevier, 1995, p. 633.
[11] P. G. Dickens, S. Crouch-Baker, and M. T. Weller, “Hydrogen insertion in oxides,” *Solid State Ionics*, vol. 18–19, no. PART 1, pp. 89–97, 1986.
[12] S. K. Deb and J. A. Chopoorian, “Optical properties and color-center formation in thin films of molybdenum trioxide,” *J. Appl. Phys.*, vol. 37, no. 13, pp. 4818–4825, 1966.
[13] K.-U. Ritzau, T. Behrendt, D. Palaferri, M. Bivour, and M. Hermle, “Hydrogen doping of Indium Tin Oxide due to thermal treatment of hetero-junction solar cells,” *Thin Solid Films*, vol. 599, pp. 161–165, 2016.
[14] J. Werner, J. Geissbühler, A. Dabirian, S. Nicolay, M. Morales-Masis, S. De Wolf, B. Niesen, and C. Ballif, “Parasitic Absorption Reduction in Metal Oxide-Based Transparent Electrodes: Application in Perovskite Solar Cells,” *ACS Appl. Mater. Interfaces*, vol. 8, no. 27, pp. 17260–17267, 2016.
[15] T. Koida, H. Fujiwara, and M. Kondo, “Hydrogen-doped In_2O_3 as high-mobility transparent conductive oxide,” *Jpn. J. Appl. Phys.*, vol. 46, no. 28, pp. 685–687, 2007.
[16] L. G. Gerling, C. Voz, R. Alcubilla, J. Puigdollers, R. Alcubilla, and J. Puigdollers, “Origin of passivation in hole-selective transition metal oxides for crystalline silicon heterojunction solar cells,” *J. Mater. Res.*, vol. 32, no. 2, pp. 260–268, 2017.
[17] M. Mews, L. Korte, and B. Rech, “Oxygen vacancies in tungsten oxide and their influence on tungsten oxide/silicon heterojunction solar cells,” *Sol. Energy Mater. Sol. Cells*, vol. 158, pp. 77–83, 2016
[18] J. Colton, A. M. Guzman, and J. W. Rabalais, “Photochromism and Electrochromism in Amorphous Transition Metal Oxide Films,” *Acc. Chem. Res.*, vol. 64, no. 1973, pp. 170–176, 1978.
[19] A. Borgschulte, O. Sambalova, R. Delmelle, S. Jenatsch, R. Hany, and F. Nüesch, “Hydrogen reduction of molybdenum oxide at room temperature,” *Sci. Rep.*, vol. 7, no. December 2016, p. 40761, 2017.
[20] E. Shanthi, a. Banerjee, V. Dutta, and K. L. Chopra, “Annealing characteristics of tin oxide films prepared by spray pyrolysis,” *Thin Solid Films*, vol. 71, no. 2, pp. 237–244, 1980.
[21] T. J. Driscoll, L. D. McCormick, and W. C. Lederer, “Altered layer formation and sputtering yields for 5 keV Ar^+ bombardment of MoO3 and WO3,” *Surf. Sci.*, vol. 187, no. 2–3, pp. 539–558, 1987.
[22] T. H. Fleisch and G. J. Mains, “An XPS study of the UV reduction and photochromism of MoO_3 and WO_3,” *J. Chem. Phys.*, vol. 76, no. 2, pp. 780–786, 1982.
[23] A. Shah, *Thin-film silicon solar cells*. EPFL press, 2010.
[24] M. Vasilopoulou, A. M. Douvas, D. G. Georgiadou, L. C. Palilis, S. Kennou, L. Sygellou, A. Soultati, I. Kostis, G. Papadimitropoulos, D. Davazoglou, and P. Argitis, “The influence of hydrogenation and oxygen vacancies on molybdenum oxides work function and gap states for application in organic optoelectronics,” *J. Am. Chem. Soc.*, vol. 134, no. 39, pp. 16178–16187, 2012.
[25] J. P. Ponpon and B. Bourdon, “Oxidation of glow discharge of a-Si:H,” *Solid. State. Electron.*, vol. 25, no. 9, pp. 875–876, 1982.
[26] N. Blayo and B. Drévillon, “Infrared ellipsometry study of the oxidation mechanisms of hydrogenated amorphous silicon,” *Surf. Sci.*, vol. 260, no. 1–3, pp. 37–43, 1992.
[27] M. C. Galetz, “Coatings for Superalloys,” in *Superalloys*, InTech, 2015.
[28] A. Atkinson, “Transport processes during the growth of oxide films at elevated temperature,” *Rev. Mod. Phys.*, vol. 57, no. 2, pp. 437–470, 1985.
[29] M. T. Greiner, L. Chai, M. G. Helander, W. M. Tang, and Z. H. Lu, “Metal/metal-oxide interfaces: How metal

contacts affect the work function and band structure of MoO_3," *Adv. Funct. Mater.*, vol. 23, no. 2, pp. 215–226, 2013.
[30] Q. Fu and T. Wagner, "Metal/oxide interfacial reactions: Oxidation of metals on $SrTiO_3$ (100) and TiO_2 (110)," *J. Phys. Chem. B*, vol. 109, no. 23, pp. 11697–11705, 2005.
[31] R. F. Egerton, "Electron energy-loss spectroscopy in the TEM," *Reports Prog. Phys.*, vol. 72, no. 1, p. 16502, 2008.
[32] L. Lajaunie, F. Boucher, R. Dessapt, and P. Moreau, "Quantitative use of electron energy-loss spectroscopy Mo-M2,3 edges for the study of molybdenum oxides," *Ultramicroscopy*, vol. 149, pp. 1–8, 2015.
[33] D. E. Diaz-Droguett, A. Zuñiga, G. Solorzano, and V. M. Fuenzalida, "Electron beam-induced structural transformations of MoO_3 and MoO_{3-x} crystalline nanostructures," *J. Nanoparticle Res.*, vol. 14, no. 1, p. 679, 2012.
[34] D. Wang, D. S. Su, and R. Schlögl, "Electron beam induced transformation of MoO3 to MoO2 and a new phase MoO," *Zeitschrift fur Anorg. und Allg. Chemie*, vol. 630, no. 7, pp. 1007–1014, 2004.
[35] C. C. Ahn and O. L. Krivanek, *EELS Atlas*. 1983.
[36] A. Illiberi, P. Kudlacek, A. H. M. Smets, M. Creatore, and M. C. M. van de Sanden, "Effect of ion bombardment on the a-Si:H based surface passivation of c-Si surfaces," *Appl. Phys. Lett.*, vol. 98, no. 24, p. 242115, 2011.
[37] B. Demaurex, J. P. Seif, S. Smit, B. Macco, W. M. M. E. Kessels, J. Geissbühler, S. De Wolf, and C. Ballif, "Atomic-Layer-Deposited Transparent Electrodes for Silicon Heterojunction Solar Cells," *IEEE J. Photovoltaics*, vol. 4, no. 6, pp. 1387–1396, 2014.
[38] S. Bowden and A. Rohatagi, "Rapid and accurate determination of series resistance and fill factor losses in industrial silicon solar cells," in *7th European Photovoltaic Solar Energy Conference and Exhibition*, 2001.
[39] J. P. Seif, A. Descoeudres, M. Filipic, F. Smole, M. Topic, Z. C. Holman, S. De Wolf, and C. Ballif, "Amorphous silicon oxide window layers for high-efficiency silicon heterojunction solar cells," *J. Appl. Phys.*, vol. 115, no. 2, 2014.